Cross section of ^{15}N-^{2}D nuclear reactions from 3.3 to 7.0 MeV for simultaneous hydrogen and deuterium quantitation in surface layers with ^{15}N ion beams

Markus Wilde[1,*], Masuaki Matsumoto[2], Liang Gao[3], Thomas Schwarz-Selinger[3], Armin Manhard[3], and Wolfgang Jacob[3]

[1] *Institute of Industrial Science, The University of Tokyo, 4-6-1 Komaba, Meguro-ku, 153-8505 Tokyo, Japan*

[2] *Tokyo Gakugei University, 4-1-1 Nukui-kita-machi, Koganei-shi, 184-8501 Tokyo, Japan*

[3] *Max-Planck Institute for Plasma Physics, Boltzmannstraße 2, D-85748 Garching, Germany*

*Corresponding author: wilde@iis.u-tokyo.ac.jp

Abstract

The cross section for the combined $^{2}D(^{15}N,p)^{16}N$ and $^{2}D(^{15}N,n\gamma)^{16}O$ nuclear reactions of deuterium (^{2}D) with incident ^{15}N ions is evaluated and found to increase by two orders of magnitude between 3.3 and 7.0 MeV. Detecting the γ-rays at 6.1 and 7.1 MeV from these reactions allows quantifying the depth-integrated ^{2}D content in materials in parallel with nanometer-resolved quantitative hydrogen (^{1}H) depth profiling in surface layers through resonant $^{1}H(^{15}N,\alpha\gamma)^{12}C$ nuclear reaction analysis (NRA) using ^{15}N ion beams. The information depth and sensitivity of ^{15}N-^{2}D NRA is estimated through energy loss simulations of the ^{15}N projectiles in the analyzed material. Good agreement of the integral ^{2}D quantitation through $^{2}D(^{15}N,p)^{16}N$ and $^{2}D(^{15}N,n\gamma)^{16}O$ NRA with ^{2}D depth profiles obtained independently via $^{2}D(^{3}He,p)^{4}He$ NRA is demonstrated at the example of ^{2}D plasma-exposed tungsten samples. The simultaneous quantitation of ^{2}D and depth-resolved ^{1}H profiling with a single ^{15}N ion beam promises application potential to investigate hydrogen-isotope exchange and diffusion processes in surface and thin buried layers.

Keywords

Nuclear reaction analysis; hydrogen; deuterium; depth profiling; isotope exchange

Published in:	Nuclear Instruments and Methods in Physics Research B **478**, 56-61 (2020)
doi:	10.1016/j.nimb.2020.05.020
Submitted:	24.03.2020
Accepted:	21.05.2020
Available online:	02.06.2020

1. Introduction

Nuclear reaction analysis (NRA) via the $^{1}H(^{15}N,\alpha\gamma)^{12}C$ reaction using ^{15}N ion beams above the 6.385-MeV energy resonance is a well-established and powerful method for nanometer-resolved depth profiling of hydrogen (^{1}H) in the near-surface region of solids [1-4]. ^{15}N-^{1}H NRA quantitatively reveals the ^{1}H depth distribution in the analyzed target by registering the emitted γ-rays as a function of the ^{15}N incidence energy. At typical beam sizes of a few mm^2, $^{1}H(^{15}N,\alpha\gamma)^{12}C$ NRA depth-selectively determines the ^{1}H content in electrical conductors as well as in insulating samples with a sensitivity of $\sim1\times10^{13}$ cm^{-2} for ^{1}H at surfaces and $\sim1\times10^{18}$ cm^{-3} (~100 ppm) ^{1}H in the bulk within several tens of minutes, irrespective of the chemical binding state of ^{1}H [5]. The technique is most elegantly performed with a scintillation detector positioned behind the target outside of the analyzing vacuum system, which provides accessibility for *in-situ* sample characterization and manipulation through surface science instrumentation [3-5]. Inherently, however, $^{1}H(^{15}N,\alpha\gamma)^{12}C$ NRA is selective only to the ^{1}H isotope. This limits the technique's versatility in situations when the target material contains both ^{1}H and ^{2}D, such as in the study of hydrogen isotope exchange processes in surface layers. The latter are of profound interest in the context of plasma-surface interactions occurring in thermonuclear fusion devices [6, 7] or for the elucidation of hydrogen transportation mechanisms across metal surfaces related to hydrogenation catalysis, hydrogen storage and purification [8-10]. Depth profiling of deuterium (^{2}D) is typically performed with $^{2}D(^{3}He,p)^{4}He$ NRA using ^{3}He ion beams of much lower energy [11], which is in turn selective for only ^{2}D. Synchronous analysis of ^{1}H and ^{2}D could hitherto only be achieved by elastic recoil detection (ERD) [12-14]. This method registers H and D recoils with in-vacuum particle detectors and often additional resolution-enhancing ion optics positioned in the forward direction [15-18], which precludes integration with ^{15}N NRA for ^{1}H, as the γ-ray detector should be placed as closely as possible to the analyzed target to provide sufficient sensitivity for ^{1}H. Thus, with the aim to expand the versatility of ^{15}N NRA towards analyzing materials that contain both ^{1}H and ^{2}D, we here describe a novel approach to quantify the ^{1}H and ^{2}D isotopes in near-surface layers simultaneously, using a single ^{15}N ion beam and the convenient γ-ray detection system of a conventional ^{15}N-^{1}H NRA setup without the need for additional particle detectors.

The ^{15}N ions of energies above 6.385 MeV used as projectiles in $^{1}H(^{15}N,\alpha\gamma)^{12}C$ NRA also induce the $^{2}D(^{15}N,p)^{16}N$ and $^{2}D(^{15}N,n\gamma)^{16}O$ reactions with ^{2}D in the target. The latter reactions release γ-rays of 6.13 and 7.12 MeV [19] that are well-separated from the 4.3-MeV γ-emission from $^{1}H(^{15}N,\alpha\gamma)^{12}C$ and easily detectable with virtually no background from natural radiation (see Figure 1 below). In contrast to the sharp energy resonance of $^{1}H(^{15}N,\alpha\gamma)^{12}C$ at 6.385 MeV, the ^{15}N-^{2}D reactions are non-resonant, hence their γ-reaction cross section varies only little within the narrow scan range (~100 keV) of incident ^{15}N energies required to obtain ^{1}H profiles within several 10 nm below a target surface with $^{1}H(^{15}N,\alpha\gamma)^{12}C$ NRA. Thus, although the ^{15}N-^{2}D reactions cannot deliver information on the ^{2}D depth location, it should be possible to perform ^{1}H depth profiling in the near-surface region with $^{1}H(^{15}N,\alpha\gamma)^{12}C$ NRA while simultaneously quantifying the integral ^{2}D content in a sample from the γ-yield at 6.13 and 7.12 MeV. Although proposed as early as 1986 by Hayashi et al. [19], who reported the relative cross section of the $^{2}D(^{15}N,p)^{16}N$ and $^{2}D(^{15}N,n\gamma)^{16}O$ reactions for ^{15}N energies from 5 to 16 MeV, this approach did not attract notable applications so far. This is likely the case because only very scarce data were reported for the ^{15}N + ^{2}D reaction cross section at ^{15}N energies below ~6.4 MeV. Knowing the ^{15}N-^{2}D reaction cross section at lower energies, however, is important to assess the sensitivity of ^{2}D detection by ^{15}N-^{2}D NRA, which

decreases as a function of depth as the ^{15}N projectiles lose energy due to electronic stopping while penetrating into the analyzed target.

Thus, in order to evaluate the 'information depth' (i.e. the sensitivity of ^{15}N ions to local D as a function of depth) of ^{15}N-^{2}D NRA, we here determine the relative cross section of the $^{2}D(^{15}N,p)^{16}N$ and $^{2}D(^{15}N,n\gamma)^{16}O$ reactions for ^{15}N energies from 3.3 to 7.0 MeV. We further develop a combined detection scheme for the 4.3-MeV γ-rays from $^{1}H(^{15}N,\alpha\gamma)^{12}C$ NRA and for those of the $^{2}D(^{15}N,p)^{16}N$ and $^{2}D(^{15}N,n\gamma)^{16}O$ reactions at 6.1 and 7.1 MeV, in order to enable synchronous ^{1}H depth profiling and quantification of ^{2}D with the same ^{15}N ion beam. To this end we also evaluate the relative intensity of the 3.7-MeV γ-ray emission arising from the simultaneously excited $^{2}D(^{15}N,\alpha\gamma)^{13}C$ reaction, which partially falls into the integration region around the 4.3-MeV γ-signal from $^{1}H(^{15}N,\alpha\gamma)^{12}C$ (Figure 1). After correcting for this ^{2}D-induced background in the γ-signal for ^{1}H detection, we demonstrate the feasibility of simultaneous near-surface ^{1}H profiling and ^{2}D quantification by ^{15}N NRA at the example of two ^{2}D plasma-exposed tungsten samples with different D depth distributions that we characterized independently by $^{2}D(^{3}He,p)^{4}He$ NRA.

2. Methods and Materials

2.1 *Ion beam and sample materials*

The $^{2}D(^{15}N,p)^{16}N$ and $^{2}D(^{15}N,n\gamma)^{16}O$ cross section measurements between 3.3 and 7.0 MeV were performed with $^{15}N^{2+}$ ion beams of 10-20 nA provided by the 5-MV van-de-Graaff tandem accelerator (NEC) in an ultra-high vacuum (UHV) chamber at the MALT microanalysis laboratory of the University of Tokyo [5]. The system is described in detail in Refs. [3-5]. In order to exclude the possibility of ^{2}D loss from the samples due to thermal desorption, the UHV chamber (base pressure if baked for typically 12-24 h at 150-200°C: 6×10^{-9} Pa) was not subjected to bake-out in the present study, resulting in a residual gas pressure of ~1×10^{-5} Pa during the NRA measurements, which were conducted with the targets at room temperature. Thin (30 nm and 275 nm) films of so-called dense deuterated amorphous carbon on Si substrates (a-C:D/Si) were used as ^{2}D targets. They were prepared on the driven electrode of a capacitively coupled low-temperature plasma from CD_4 precursor gas (purity 99.5 at.%) at an operating pressure of 2 Pa and a dc-self bias of -300 V. The ^{2}D contents in the two films were determined with $^{2}D(^{3}He,p)^{4}He$ NRA using ^{3}He with 690 keV, applying the cross section of Wielunska et al. [20], to be 1.22×10^{17} cm^{-2} and 1.25×10^{18} cm^{-2} D, respectively. According to SRIM [21] and the stopping power it provided for the present composition (dE/dx = 1.85 keV/nm), the energy loss of the ^{15}N ions in the 30-nm a-C:D films is approximately constant (~56 keV) between 3.3 and 7.0 MeV. At each of the fixed incident ^{15}N energies set in increments of ~200 keV, a series of 10 consecutive measurements with beam exposures for 20 s (a total charge dose of 1-2 μC) was acquired on an initially non-irradiated spot on the C:D/Si targets (size 10 × 30 × 0.8 mm^2) after adjusting the target position relative to the ion beam (collimated and focused into a rectangular profile of 4 × 1.5 mm^2) with a μm-controlled manipulator. In each series, the γ-yield decayed slightly (by ~10%) during accumulation of the ^{15}N ion dose due to irradiation-induced loss of ^{2}D. On one of the two 30-nm a-C:D/Si targets, an additional thin film of ~10 nm (estimated, quartz microbalance) Au was deposited in the hope to suppress the degradation, but no improvement of the γ-yield stability relative to the bare a-C:D film was found in presence of the Au-coating. The γ-yield decay curves were fitted by exponential functions and extrapolated to zero ^{15}N

exposure to extract the γ-yield corresponding to the original ^{2}D content in the unperturbed a-C:D film. The ^{1}H sensitivity of ^{1}H(^{15}N,αγ)^{12}C NRA was calibrated in the same way using Kapton ($C_{22}H_{10}N_2O_5$) foil as ^{1}H-concentration standard (Dupont-Toray EN30, density: 1.45 g cm^{-3}, ^{1}H content: 2.28×10^{22} cm^{-3}, stopping power: dE/dx = 1.2879 keV/nm for ^{15}N at ~6.4 MeV) [5].
Two mirror-polished (electro polished according to Ref. [22]), polycrystalline, hot-rolled W samples, 15 × 12 × 0.7 mm^3 in size, were exposed at 300 K to a quantified low-temperature plasma source [23] after annealing in vacuum at 1200 K for 2 h. *Ex-situ* ^{2}D depth profiling was conducted afterwards with ^{2}D(^{3}He,p)^{4}He NRA in Garching. See Ref. [24] for details about the plasma exposure, the ^{2}D depth profiling, and the motivation behind the exposure.

2.2. *γ-Spectra from ^{15}N nuclear reactions with ^{1}H and ^{2}D*

The γ-rays emitted from the ^{15}N-excited nuclear reactions were registered with a 4 in. $Bi_4Ge_3O_{12}$ (BGO) scintillation detector placed on the beam axis 30 mm downstream from the target outside of the analytic vacuum chamber [3-5]. The detector output subjected to amplification by a photomultiplier and pulse height analysis with a digital multichannel analyzer (MCA) is shown in Figure 1 for the impact of MeV-^{15}N ions onto targets that contain either only ^{1}H (a) or only ^{2}D (b).

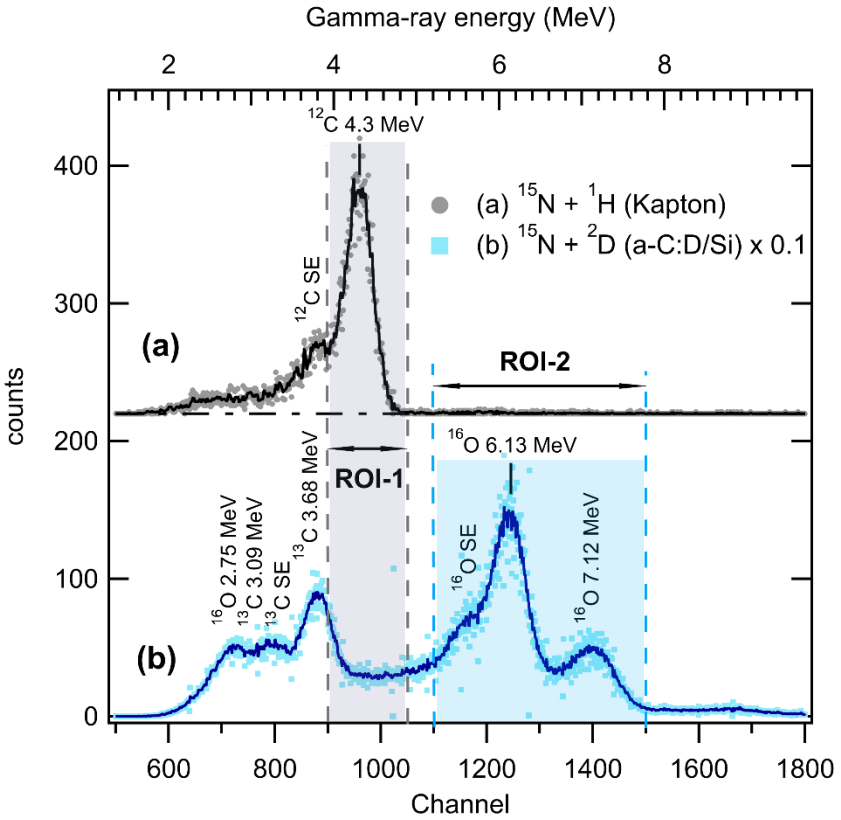

Figure 1 (color online): Typical γ-spectra from MeV-^{15}N-induced nuclear reactions with (a) ^{1}H and (b) ^{2}D. Symbols indicate raw data; solid lines are the same data smoothed twice by a binominal algorithm to reduce noise and facilitate identification of peak positions. For clarity, spectrum (a) is shifted vertically by +220 counts as indicated by the dash-dotted baseline, and spectrum (b) is scaled by a factor of 0.1. See text for peak assignments.

Spectrum (a), recorded with a dose of 7.2 μC of $^{15}N^{2+}$ at 6.54 MeV on Kapton, only shows the familiar γ-emission at 4.3 MeV (from the excited $^{12}C^*$ state produced in the $^{1}H(^{15}N,\alpha\gamma)^{12}C$ reaction) and the associated weaker single escape (SE) peak at 0.511 MeV lower energy [4, 25]. The ^{2}D-induced γ-emissions at 2.75, 6.13 and 7.12 MeV seen in spectrum (b), obtained with 8.7 μC of $^{15}N^{2+}$ at 6.385 MeV on a thicker (275 nm) film of a-C:D/Si, originate from $^{16}O^*$ excited states produced in the $^{2}D(^{15}N,p)^{16}N$ and $^{2}D(^{15}N,n\gamma)^{16}O$ reactions, which occur simultaneously [19]. The ^{16}N nucleus formed in the $^{2}D(^{15}N,p)^{16}N$ reaction is unstable and β-decays with a half-life of 7.1 s into the same $^{16}O^*$ states as those directly produced by $^{2}D(^{15}N,n\gamma)^{16}O$.

By measuring the γ-yield at 6.13 and 7.12 MeV while the ^{15}N beam irradiates the target, a combined cross section for the $^{2}D(^{15}N,p)^{16}N$ and $^{2}D(^{15}N,n\gamma)^{16}O$ reactions is thus determined. Evaluating the $^{2}D(^{15}N,p)^{16}N$ reaction cross section separately (from the delayed γ-emission due to β-decay of ^{16}N after shutting off the ^{15}N beam [19]) was not of practical interest to our present purpose and hence not pursued. The additional γ-emissions at 3.09 and 3.68 MeV seen in spectrum (b) originate from $^{13}C^*$ excited nuclear states formed in the $^{2}D(^{15}N,\alpha\gamma)^{13}C$ reaction that also occurs in parallel with $^{2}D(^{15}N,p)^{16}N$ and $^{2}D(^{15}N,n\gamma)^{16}O$ [19].

The regions of interest (ROI) between the two pairs of dashed vertical lines denoted as ROI-1 (Channel 900 – 1050) and ROI-2 (Channel 1100 – 1500) in Figure 1 indicate the energy integration intervals to extract the yields of 4.3-MeV γ-rays from $^{1}H(^{15}N,\alpha\gamma)^{12}C$ and of the 6.1 and 7.1 MeV γ-rays from $^{2}D(^{15}N,p)^{16}N$ and $^{2}D(^{15}N,n\gamma)^{16}O$, respectively, from the MCA spectrum. The accumulated γ-yields in these intervals are proportional to the respective concentrations of the ^{1}H and ^{2}D isotopes in analyzed targets. Standard $^{1}H(^{15}N,\alpha\gamma)^{12}C$ NRA is usually performed with only ROI-1. We upgraded our acquisition software in the present work to additionally provide ROI-2, in order to enable simultaneous detection of ^{1}H and ^{2}D.

Observe from spectrum (a) that ROI-2 for ^{2}D detection is virtually free of any background, even in the presence of ^{1}H in the specimen. Spectrum (b), on the other hand reveals that some γ-yield from the ^{2}D reactions, in particular a fraction of the 3.68-MeV γ-emission from $^{2}D(^{15}N,\alpha\gamma)^{13}C$, falls into ROI-1 for ^{1}H detection. The lower boundary of ROI-1 (Channel 900) was chosen such as to exclude the ^{2}D-derived 3.68-MeV γ-ray as far as possible, which already sacrifices ~25% of the 4.3-MeV γ-ray yield contained in the ^{12}C SE peak [25] and thereby somewhat lowers the NRA sensitivity for ^{1}H detection. Nonetheless, an appreciable γ-yield from the ^{15}N-^{2}D reactions remains in ROI-1, which effectively imposes a D-derived background to the 4.3-eV γ-signal from $^{1}H(^{15}N,\alpha\gamma)^{12}C$ if the target contains ^{2}D in addition to ^{1}H. The D-derived γ-yield in ROI-1 is proportional to the ^{2}D content in the target and to the ^{15}N energy-dependent $^{2}D(^{15}N,p)^{16}N$ and $^{2}D(^{15}N,n\gamma)^{16}O$ cross-section and has to be subtracted from the γ-yield detected in ROI-1 in order to quantify ^{1}H in the presence of ^{2}D. Fortunately, this ^{2}D-induced background in ROI-1 turns out to be a constant fraction of the reaction yield from the 6.1 and 7.1 MeV γ-rays detected in ROI-2 (see Figure 3 below) and is hence straightforward to evaluate and correct for.

3. Results and Discussion

3.1. *Cross section of $^{2}D(^{15}N,p)^{16}N$ and $^{2}D(^{15}N,n\gamma)^{16}O$*

The initial γ-yield at 6.1 and 7.1 MeV from the $^{2}D(^{15}N,p)^{16}N$ and $^{2}D(^{15}N,n\gamma)^{16}O$ reactions for ^{15}N ions incident onto the 30-nm thin a-C:D films with energies between 3.3 to 7.0 MeV is shown in Figure 2. The plotted ^{15}N energies are those provided by the accelerator after correcting for ½ of the energy loss in the 30 nm a-C:D film (28 keV, i.e., mid-film) and, where applicable, for the additional stopping loss of 33-40 keV in the 10 nm Au cover layer. The respective ^{15}N stopping losses were determined by SRIM simulations for all incidence energies. For simplicity, and to accommodate any uncertainties in film thicknesses and stopping powers, horizontal error bars were (generously) estimated by 28 keV, which is larger than the energy spread of the incident ^{15}N ion beam (~1.6-3.3 keV) and straggling in both layers (7-8 keV (Au) + 4.5 keV (a-C:D)) combined. The measured 6.1 and 7.1-MeV γ-yield data are expressed as a relative cross section after normalizing to the yield obtained at 6.52 MeV, which is a typical ^{15}N energy for near-surface ^{1}H depth profiling with $^{1}H(^{15}N,\alpha\gamma)^{12}C$ NRA that corresponds to a probing depth of 34 nm in tungsten (W, d*E*/d*x* = 4.01 keV/nm for ~6.4 MeV ^{15}N). Vertical error bars reflect the γ-ray counting statistics [5]. The relative errors increase at lower ^{15}N energies due to diminishing ion beam output from the accelerator and smaller counting rates due to the declining cross section.

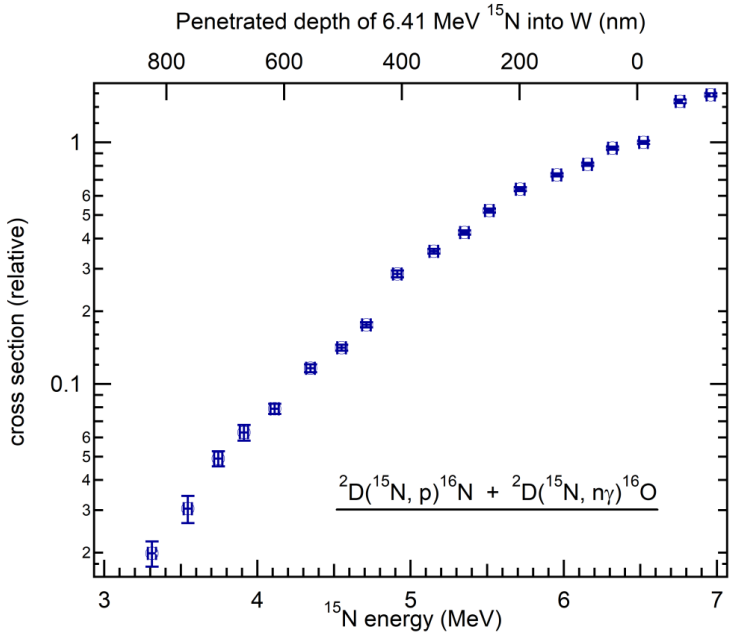

Figure 2 (color online): Cross section of the $^{2}D(^{15}N,p)^{16}N$ and $^{2}D(^{15}N,n\gamma)^{16}O$ reactions from 3.3 to 7.0 MeV. The upper abscissa indicates the depth in tungsten (W), at which the residual energy of a ^{15}N ion incident at 6.41 MeV falls to the values on the lower energy abscissa due to electronic stopping. The energy-depth correlation was determined by a SRIM [21] simulation.

Figure 2 indicates that the relative ^{15}N-^{2}D cross section increases by two orders of magnitude between 3.3 and 7.0 MeV. The energy dependence of the relative cross section obtained here connects well with data in the range from 5 to 16 MeV reported by Hayashi et al. [19] (see Supplementary Material S1), which show that the cross section increases further (about 2.5 times) between 7 and 16 MeV. Certain step-like variations of the cross-section appear around

~4.8 and ~6.6 MeV, which may correspond to excited nuclear states encountered in the ^{15}N-^{2}D reactions, but no pronounced resonances are seen in the entire range from 3.3 to 7.0 MeV. These observations are also consistent with Ref. [19]. The strongly non-linear cross section increase around 6.6 MeV is not considered to be experimental error and was reproduced by detailed ^{15}N-^{2}D NRA measurements in the energy range of 6.4 – 7.3 MeV that shall be reported in a forthcoming publication [26].

To assess the 'information depth' (i.e., the depth-dependent sensitivity) of ^{2}D detection during simultaneous near-surface ^{1}H profiling with ^{1}H(^{15}N,αγ)^{12}C NRA for the case of tungsten (W), we simulated the trajectories of initially 6.41-MeV ^{15}N ions in W with SRIM. In ^{15}N-^{1}H NRA, ^{15}N ions incident at 6.41 MeV probe ^{1}H in W in a shallow near-surface depth of 6 nm. The simulations show that these 6.41-MeV ^{15}N ions are slowed down in tungsten to 3.3 MeV in a depth of ~820 nm, which is indicated by the upper abscissa in Figure 2 (between 3.3 and 7.0 MeV the ^{15}N stopping power is near the Bragg peak maximum and almost constant). Figure 2 thus reveals that due to the rather slow decrease of the cross section towards lower ^{15}N energy the ^{15}N-^{2}D nuclear reactions probe ^{2}D even in ~820 nm depth with still ~2% of the sensitivity they provide for ^{2}D near the surface.

In order to determine the magnitude of ^{2}D-induced background in ROI-1 that interferes with ^{1}H detection via ^{1}H(^{15}N,αγ)^{12}C NRA, we monitored the ^{2}D-derived γ-yield in ROI-1 during the ^{15}N-^{2}D reaction cross section measurements with the a-C:D film targets, which only contain a negligible amount of ^{1}H in their volume. Figure 3 shows that the ^{2}D-derived γ-yield in ROI-1 (mainly the 3.7-MeV γ-ray from ^{2}D(^{15}N,pγ)^{13}C) assumes an approximately constant fraction of 20.3 ± 2.3 % of the γ-yield detected in ROI-2 (the 6.1 + 7.1 MeV γ-emissions from ^{2}D(^{15}N,p)^{16}N and ^{2}D(^{15}N,nγ)^{16}O) in the entire energy region from 3.3 to 7.0 MeV. Knowledge of this ratio allows for a facile correction of the ^{2}D-induced background in ROI-1 on the basis of the measured ^{2}D γ-yield in ROI-2, thus enabling quantitative ^{1}H depth profiling also in targets that contain the ^{2}D isotope. An exception is the higher value of 25 ± 1.5% near ~6.385 MeV, which is likely caused by ^{1}H-containg contaminants adsorbed on the target surface that also produced a measureable 4.3-MeV γ-yield in ROI-1.

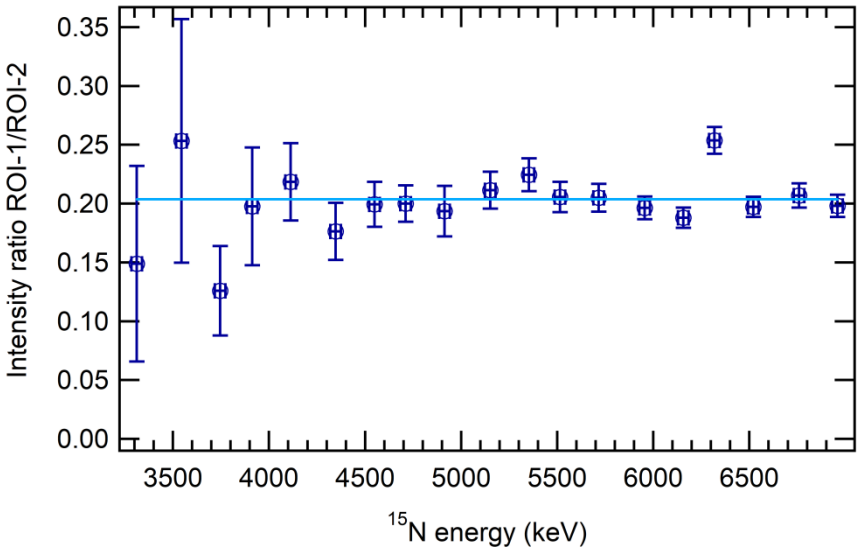

Figure 3 (color online): Intensity ratio of ^{15}N-^{2}D-induced γ-emissions in ROI-1 (~4.3 MeV) and ROI-2 (6.1 + 7.1 MeV) for ^{15}N energies from 3.3 to 7.0 MeV.

3.2. *Simultaneous ^{1}H and ^{2}D Quantification with ^{15}N NRA*

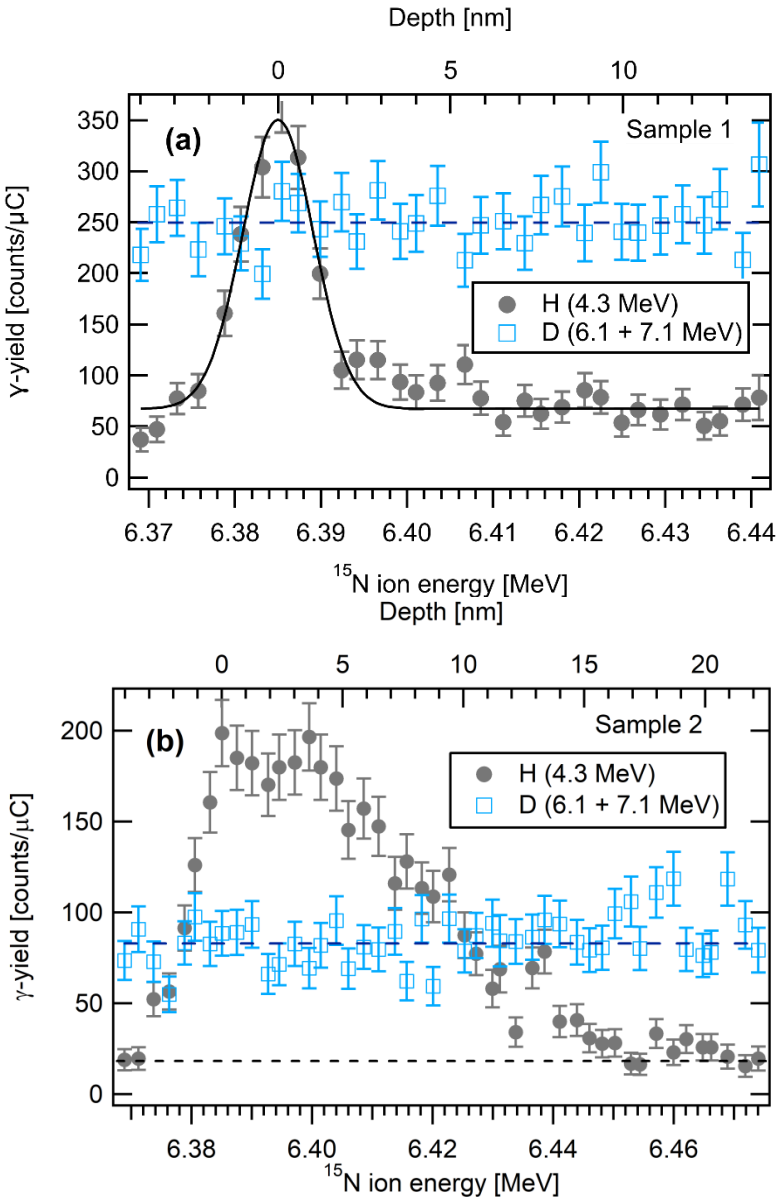

Figure 4 (color online): (a) ^{15}N-^{1}H NRA profile (full circles) from Sample 1 (^{2}D plasma-exposed tungsten) showing a peak at 6.385 MeV from surface-adsorbed ^{1}H on a plateau of ^{2}D-induced γ-yield. Open squares: simultaneously recorded γ-yield from the ^{15}N-^{2}D reactions. (b) ^{15}N ^{1}H NRA profile (full circles) from Sample 2 (first ^{2}D plasma- and then ^{1}H plasma-exposed tungsten) showing a ~10 nm thick ^{1}H-rich surface layer and less γ-yield of ^{2}D-derived γ-rays at 6.1 and 7.1 MeV (open squares) than Sample 1.

Exemplifying the simultaneous quantification of ^{1}H and ^{2}D through combined ^{1}H and ^{2}D NRA with ^{15}N, we present in Figure 4 NRA profiles of the two ^{2}D plasma-exposed tungsten targets. Sample 1 was only exposed to a ^{2}D fluence of 6×10^{24} D m^{-2} with the target biased to reach a maximum ion energy of 215 eV, whereas sample 2 was subsequently treated in addition with ^{1}H-plasma at a lower ion energy of only 15 eV to the same fluence of 6×10^{24} D m^{-2} in order to partially exchange ^{2}D against ^{1}H in the near-surface region. Figure 4 (a)

shows the highly depth-resolved NRA ^{1}H profile and the ^{2}D-induced γ-yield from Sample 1, revealing a typical Gaussian-shaped peak at the 6.385 MeV resonance energy of the ^{1}H(^{15}N,αγ)^{12}C reaction, indicative of ^{1}H adsorbed on the sample surface with a coverage of $(2.2 \pm 0.3)\times10^{15}$ cm^{-2} as determined from the peak integral. The surface peak sits on a γ-yield plateau of 67.5 ± 3.2 cts/μC, which amounts to ~24% of the ^{2}D-derived yield of 6.1 + 7.1-MeV γ-rays of averaged 250.9 ± 25.0 cts/μC. This plateau height corresponds exactly to the relative ^{2}D-induced background level expected from Figure 3 near 6.385 MeV, suggesting that the γ-yield plateau detected in ROI-1 consists predominantly of ^{2}D-derived background from the ^{15}N-^{2}D reactions and thus that the sample does not actually contain a sizeable quantity of ^{1}H below the surface, which is well consistent with the sample history (only ^{2}D plasma-exposed and air-transported).

The ^{15}N-^{2}D yield of 6.1 + 7.1 MeV γ-rays reflects the total depth-integrated amount of ^{2}D in the near-surface region, i.e., the ^{2}D(^{15}N,p)^{16}N and ^{2}D(^{15}N,nγ)^{16}O cross section convolved with the ^{2}D depth distribution. The ^{2}D depth profile of Sample 1 determined by ^{2}D(^{3}He,p)^{4}He NRA is shown in Figure 5, which indicates a ~10 nm thick ^{2}D-rich surface layer (^{2}D concentration: 10 at. %) [24] and a total ^{2}D content of 1.84×10^{16} cm^{-2} in the top 820 nm. Neglecting ^{2}D in even deeper regions and numerically convolving the relative cross section in Figure 2 with the ^{3}He-^{2}D depth profile up to 820 nm and comparing the integral to the absolute γ-yields measured from the 30-nm a-C:D film target that contained 1.22×10^{17} ^{2}D cm^{-2} leads to an expected 6.1+7.1 MeV γ-yield of 340 cts/μC (± ~15%), which is only slightly larger than our experimentally observed value of 257 ± 29.0 cts/μC (average of two ^{1}H + ^{2}D profiles from Sample 1 (only one of these is shown in Figure 4(a)).

The ^{15}N NRA ^{1}H profile of Sample 2 in Figure 4 (b) shows a ~10 nm wide ^{1}H-rich surface layer with a plateau-like distribution in the topmost 5 nm after the additional low-energy H-plasma treatment. Compared with the data of Sample 1 in Figure 4 (a), the ^{2}D-derived yield of 6.1 + 7.1-MeV γ-rays is reduced to an average of 85.1 ± 13.6 cts/μC (long-dashed line) and the ^{2}D-induced background plateau underneath the ^{1}H profile (short-dashed line) amounts to only 20.4 ± 3.3 cts/μC. The latter two intensities again reproduce the ~25% intensity ratio of ROI-1/ROI-2 near 6.385 MeV in Figure 3, indicating that the ^{1}H concentration in Sample 2 decreases to the detection limit in depths beyond 15 nm, i.e., ^{1}H exists only in the ~10 nm thin ^{1}H-rich surface layer, where it attains a maximum concentration of $(5.0 \pm 1.0)\times10^{21}$ cm^{-3} (8.0 ± 1.7 at.% of the W atomic density) in the topmost 5 nm as judged from the averaged γ-yield (183.2 ± 9.4 cts/μC) after subtraction of the ^{2}D-induced background. These results suggest that a large part of ^{2}D initially present in the near-surface region of Sample 1 was replaced by ^{1}H during the additional low-energy ^{1}H-plasma treatment. This is clearly confirmed by the ^{2}D depth profile of Sample 2 obtained with ^{3}He-^{2}D NRA shown for comparison in Figure 5. Convolving again the top 820 nm of this ^{2}D profile with the relative ^{15}N-^{2}D cross section and comparing the integral to the absolute ^{2}D-derived γ-yield measured on the 30-nm a-C:D films lets us expect a 6.1+7.1 MeV γ-yield of 82.7 cts/μC (± ~15%), which agrees quantitatively with the experimental value of 78.7 ± 13.2 cts/μC (the averaged results of two ^{1}H + ^{2}D profiles from Sample 2; only one of these is shown in Figure 4(b)).

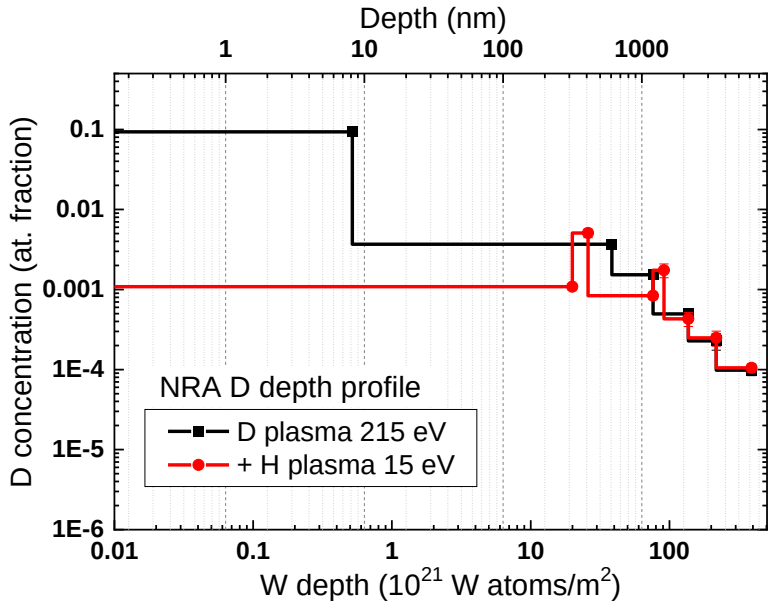

Figure 5 (color online): ^{2}D Depth profiles obtained by ^{2}D(^{3}He,p)^{4}He NRA from Sample 1 (exposed to ^{2}D plasma, 215 eV) and Sample 2 (additionally ^{1}H plasma, 15 eV).

Our results represent the first successful simultaneous quantification of ^{1}H and ^{2}D in the near-surface region with a single ^{15}N ion beam and demonstrate satisfactory agreement with independently performed ^{2}D depth profiling *via* ^{2}D(^{3}He,p)^{4}He NRA. In order to enable our readers to perform ^{2}D quantitation by numerical convolution, we provide the numerical values of the energy-dependent cross section (Figure 2) in Supplementary Materials S2. In view of Figure 2, the sensitivity of ^{15}N-^{2}D NRA for ^{2}D is evidently energy-dependent, i.e., it varies strongly with both the incident ^{15}N energy and with the depth location of ^{2}D in the sample. Comparing the absolute sensitivities to detect an atomic monolayer (ML) density (1.0×10^{15} cm^{-2}) of ^{1}H or ^{2}D on a surface with ^{15}N at 6.385 MeV, we note that the ^{1}H(^{15}N,$\alpha\gamma$)^{12}C reaction typically produces 4.3 MeV γ-yields of ~100 cts/μC, whereas the yield from ^{15}N-^{2}D NRA is ~3 times smaller (30.2 cts/μC). The method is hence particularly suited to target materials that contain moderately large quantities of ^{2}D (several MLs) confined to thin near-surface layers. An inherent weakness of the proposed approach is the ambiguity to interpret a given γ-yield from the ^{2}D(^{15}N,p)^{16}N and ^{2}D(^{15}N,nγ)^{16}O reactions when the actual ^{2}D depth distribution in the sample is entirely unknown and may extend over large depth ranges. Decreased ^{2}D-derived γ-yield, for instance, may then arise either from ^{2}D loss from the target (such as from desorption or ^{1}H/^{2}D isotope exchange) as well as from a redistribution of ^{2}D into deeper bulk regions, where the probing ^{15}N energy is reduced by stopping and hence the effective ^{15}N-^{2}D cross section smaller. The ^{15}N-^{2}D NRA method should nonetheless be useful whenever the depth location of the ^{2}D in the sample is rigidly confined to a narrow depth region by the target material and structure in the depth dimension, such as in the present case of the thin a-C:D films, where the ^{2}D solubility in the Si substrates is far below the NRA detection limit [27]. For similar such systems, we therefore expect the method to be highly promising to investigate ^{1}H/^{2}D exchange or diffusion processes in surface thin films or in buried thin layers of ^{1}H/^{2}D-containing functional materials by means of isotopic tracing.

4. Conclusions

A detection scheme was developed for the 6.1 and 7.1-MeV γ-rays from the $^{2}D(^{15}N,p)^{16}N$ and $^{2}D(^{15}N,n\gamma)^{16}O$ reactions in parallel with the 4.3-MeV γ-emission from $^{1}H(^{15}N,\alpha\gamma)^{12}C$. The combined cross section for the $^{15}N + ^{2}D$ reactions increases by two orders of magnitude from 3.3 to 7.0 MeV without pronounced resonances. The ^{2}D sensitivity of ^{15}N-^{2}D NRA at 6.4 MeV is ~30% of the one $^{1}H(^{15}N,\alpha\gamma)^{12}C$ NRA provides for ^{1}H near the surface and decreases with depth in the analyzed target due to ^{15}N stopping as assessable with SRIM simulations. Convolving the ^{15}N-^{2}D reaction cross section with the ^{2}D depth distribution and integration allows quantifying the ^{2}D content in the near-surface region of targets. The parallel measurement of ^{1}H depth profiles and quantification of the depth-integrated ^{2}D content with a single ^{15}N ion beam is considered versatile to investigate ^{1}H-^{2}D isotope exchange and diffusion processes in surface-near layers of systems where the ^{2}D location is known or reasonably assumed, e.g., in targets where material and geometry confine the ^{2}D distribution to a narrow depth region, such as thin deuterated films on nearly ^{2}D-free substrates or thin buried layers of ^{2}D containing functional materials.

Declaration of Competing Interest

The authors declare that they have no known competing financial interests or personal relationships that could have appeared to influence the work reported in this paper.

Acknowledgements

M. W. would like to thank H. Matsuzaki and H. Tokuyama for technical assistance in the MALT accelerator operation. This work was supported by the Institute of Industrial Science, The University of Tokyo, and by the Max-Planck-Institute for Plasma Physics, Garching. This research did not receive any specific grant from funding agencies in the public, commercial, or not-for-profit sectors.

5. References

[1] W.A. Lanford, H.P. Trautvetter, J.F. Ziegler, J. Keller, New precision technique for measuring concentration versus depth of hydrogen in solids, Appl. Phys. Lett. 28 (1976) 566-568.

[2] W.A. Lanford, Nuclear Reactions for Hydrogen Analysis, in: J.R. Tesmer, M. Nastasi (Eds.) Handbook of Modern Ion Beam Materials Analysis, Materials Research Society, Pittsburgh, PA, 1995, pp. 193-204.

[3] K. Fukutani, Below-surface behavior of hydrogen studied by nuclear reaction analysis, Curr. Op. Solid State Mat. Sci. 6 (2002) 153-161.

[4] M. Wilde, K. Fukutani, Hydrogen detection near surfaces and shallow interfaces with resonant nuclear reaction analysis, Surf. Sci. Rep. 69 (2014) 196-295.

[5] M. Wilde, S. Ohno, S. Ogura, K. Fukutani, H. Matsuzaki, Quantification of Hydrogen Concentrations in Surface and Interface Layers and Bulk Materials through Depth Profiling with Nuclear Reaction Analysis, J. Vis. Expt. (2016) e53452.

[6] R. Behrisch, Measurement of Hydrogen Isotopes in Plasma-facing Materials of Fusion Devices, Phys. Scr. T94 (2001) 52.

[7] P. Petersson, J. Jensen, A. Hallén, G. Possnert, Measurement of hydrogen isotopes by a nuclear microprobe, J. Phys.: Conf. Ser. 100 (2008) 062029.

[8] S. Ohno, M. Wilde, K. Fukutani, Novel insight into the hydrogen absorption mechanism at the Pd(110) surface, The J. Chem. Phys. 140 (2014) 134705.

[9] S. Ohno, M. Wilde, K. Mukai, J. Yoshinobu, K. Fukutani, Mechanism of Olefin Hydrogenation Catalysis Driven by Palladium-Dissolved Hydrogen, J. Phys. Chem. C 120 (2016) 11481-11489.

[10] M. Wilde, K. Fukutani, Penetration mechanisms of surface-adsorbed hydrogen atoms into bulk metals: Experiment and model, Phys. Rev. B 78 (2008) 115411.

[11] M. Mayer, E. Gauthier, K. Sugiyama, U. von Toussaint, Quantitative depth profiling of deuterium up to very large depths, Nucl. Instrum. Methods Phys. Res. B 267 (2009) 506-512.

[12] R. Pretorius, M. Peisach, J.W. Mayer, Hydrogen and deuterium depth profiling by elastic recoil detection analysis, Nucl. Instrum. Methods Phys. Res. B 35 (1988) 478-483.

[13] S. Markelj, O.V. Ogorodnikova, P. Pelicon, T. Schwarz-Selinger, K. Sugiyama, I. Čadež, Study of thermal hydrogen atom interaction with undamaged and self-damaged tungsten, J. Nucl. Mater. 438 (2013) S1027-S1031.

[14] S. Markelj, A. Založnik, T. Schwarz-Selinger, O.V. Ogorodnikova, P. Vavpetič, P. Pelicon, I. Čadež, In situ NRA study of hydrogen isotope exchange in self-ion damaged tungsten exposed to neutral atoms, J. Nucl. Mater. 469 (2016) 133-144.

[15] O. Kruse, H.D. Carstanjen, High depth resolution ERDA of H and D by means of an electrostatic spectrometer, Nucl. Instrum. Methods Phys. Res. B 89 (1994) 191-199.

[16] F. Schiettekatte, A. Chevarier, N. Chevarier, A. Plantier, G.G. Ross, Quantitative depth profiling of light elements by means of the ERD E × B technique, Nucl. Instrum. Methods Phys. Res. B 118 (1996) 307-311.

[17] K. Kimura, K. Nakajima, S. Yamanaka, M. Hasegawa, H. Okushi, Hydrogen depth-profiling in chemical-vapor-deposited diamond films by high-resolution elastic recoil detection, Appl. Phys. Lett. 78 (2001) 1679-1681.

[18] G. Dollinger, A. Bergmaier, L. Goergens, P. Neumaier, W. Vandervorst, S. Jakschik, High resolution elastic recoil detection, Nucl. Instrum. Methods Phys. Res. B 219-220 (2004) 333-343.

[19] S. Hayashi, H. Nagai, M. Aratani, T. Nozaki, M. Yanokura, I. Kohno, O. Kuboi, Y. Yatsurugi, High sensitivity analysis of deuterium in solids by 15N-induced nuclear reactions, Nucl. Instrum. Methods Phys. Res. B 16 (1986) 377-382.

[20] B. Wielunska, M. Mayer, T. Schwarz-Selinger, U. von Toussaint, J. Bauer, Cross section data for the D(^{3}He,p)^{4}He nuclear reaction from 0.25 to 6 MeV, Nucl. Instrum. Methods Phys. Res. B 371 (2016) 41-45.

[21] J. Ziegler, J.P. Biersack, M.D. Ziegler, SRIM – The stopping and ranges of ions in matter, http://www.srim.org/, retrieved 3/23/2020.

[22] A. Manhard, G. Matern, M. Balden, A Step-By-Step Analysis of the Polishing Process for Tungsten Specimens, Practical Metallography 50 (2013) 5-16.

[23] A. Manhard, T. Schwarz-Selinger, W. Jacob, Quantification of the deuterium ion fluxes from a plasma source, Plasma Sources Sci. Technol. 20 (2011) 015010.

[24] L. Gao, W. Jacob, U.v. Toussaint, A. Manhard, M. Balden, K. Schmid, T. Schwarz-Selinger, Deuterium supersaturation in low-energy plasma-loaded tungsten surfaces, Nucl. Fusion 57 (2017) 016026.

[25] K.M. Horn, W.A. Lanford, Suppression of background radiation in BGO and NaI detectors used in nuclear reaction analysis, Nucl. Instrum. Methods Phys. Res. B 45 (1990) 256-259.

[26] M. Wilde, T. Chikada, W. Mao, to be published, (2020).

[27] A. Van Wieringen, N. Warmoltz, On the permeation of hydrogen and helium in single crystal silicon and germanium at elevated temperatures, Physica 22 (1956) 849-865.